Published by Institute of Physics Publishing for SISSA/ISAS

Received: *November 6, 2002*
Revised: *December 2, 2002*
Accepted: *December 3, 2002*

Landau-Pomeranchuk-Migdal resummation for dilepton production*

Patrick Aurenche

Laboratoire d'Annecy-le-Vieux de Physique Théorique, B.P. 110
UMR 5108 du CNRS associée à l'Université de Savoie
74941 Annecy-le-Vieux Cedex, France
E-mail: aurenche@lapp.in2p3.fr

François Gelis

Service de Physique Théorique, Bat. 774, CEA/Saclay
91191, Gif-sur-Yvette Cedex, France
E-mail: gelis@spht.saclay.cea.fr

Guy David Moore

Department of Physics, University of Washington
Seattle, Washington 98195, USA, and
Department of Physics, McGill University
3600 rue University, Montréal QC H3A 2T8, Canada
E-mail: guymoore@phys.washington.edu

Haitham Zaraket

Physics Department, University of Winnipeg
Winnipeg, Manitoba R3B 2E9, Canada
E-mail: zaraket@lapp.in2p3.fr

Abstract: We consider the thermal emission rate of dileptons from a QCD plasma in the small invariant mass ($Q^2 \sim g_s^2 T^2$) but large energy ($q^0 \gtrsim T$) range. We derive an integral equation which resums multiple scatterings to include the LPM effect; it is valid at leading order in the coupling. Then we recast it as a differential equation and show a simple algorithm for its solution. We present results for dilepton rates at phenomenologically interesting energies and invariant masses.

Keywords: Thermal Field Theory, QCD.

*A test program calculating the LPM corrections to the photon and dilepton rates can be found at the URL: http://www-spht.cea.fr/articles/T02/150/libLPM/

JHEP12(2002)006

Contents

1. Introduction

In the last few years progress has been achieved in understanding the production of electromagnetic probes in a quark-gluon plasma in equilibrium. In the case of a hard photon (which is defined as having an energy larger than the temperature T of the plasma) the usual Compton and annihilation processes discussed long ago [1, 2] are not the only leading-order mechanisms. It turns out that bremsstrahlung of a quark in a plasma gives a leading contribution [3, 4] and, more importantly, a crossed process from bremsstrahlung actually dominates at a large enough energy [5]–[8]. This process, sometimes referred to as off-shell annihilation or annihilation with scattering, is of type 3-*body* $\to$ 2-*body*: the photon is produced via quark-antiquark annihilation where one of the incoming quarks is put off-shell by scattering in the plasma. However, the formation time of the photon is comparable to, or larger than, the average time between soft scatterings of a quark in the plasma (inverse of the damping rate). This implies that multiple scattering plays an important role in these photon emission processes [9].

A correct treatment of multiple scattering, even after performing Hard Thermal Loop (HTL) resummation [10], involves the resummation of ladder diagrams with effective propagators for both fermions and gluons. This resummation leads to an integral equation, which has been solved to give the photon emission rate to leading order in the strong coupling g_s [11, 12, 13]. The resummation of higher loop diagrams implements the Landau-

Pomeranchuk-Migdal [14, 15, 16] effect which has been much discussed recently in the context of jet energy loss in a hot medium [17]–[22]. However, there are differences between the approach followed here for photon production and that used for jet quenching: we work consistently in the HTL approach, using the actual distribution of moving charges in the plasma and dynamical screening of interactions, rather than a model of static, Debye screened charges. Note that no magnetic mass needs to be introduced in order to screen transverse gluons, since ultrasoft divergences have been shown to cancel thanks to cancellations between diagrams of different topologies [11] (see also [23]–[26]).

Preliminary hydrodynamical studies [27]–[31], which take into account the above mechanisms of photon production, show that the thermal rate (including the contribution from the hot hadronic phase) should clearly emerge above prompt photon sources (produced in the early stages of the collisions) in a range from 1 GeV – 3 GeV to 5 GeV at RHIC and LHC.

The above developments are quite timely in view of the recent WA98 measurements at SPS [32] and of the upcoming results at RHIC where the photon spectrum in gold-gold collisions is being measured [33]. There is however an uncertainty concerning the possibility of separating the spectrum of direct photons from that of photons which are decay products of resonances, in particular π^0's. In the energy range of interest the π^0 signal may be almost two orders of magnitude above the direct photon rate and the subtraction of the π^0, η, ... background from the data is a formidable experimental challenge.

In the mean time it is interesting to consider an alternative channel which carries the same dynamical information as the real photon production rate, but which suffers a different, less important, background. This is the case of the production of low mass lepton pairs at large momentum. The invariant mass of the pair should be high enough to be above the background of Dalitz pairs from the pions, but small enough that the rate remains appreciable. Typically one expects the range 150 Mev $< \sqrt{Q^2} < 500\,\mathrm{MeV}$ to be realistic for our purposes ($\sqrt{Q^2}$ is the invariant mass of the lepton pair). Higher mass ranges (above the vector meson masses) should also be explored.

This rate has already been calculated for the Drell-Yan process [34], for the $2 \to 2$ processes [35, 36], and for bremsstrahlung and off-shell annihilation in the approximation where the quark undergoes a single scattering in the medium [37]. The analysis of multiple scattering is clearly called for. Compared to the real photon case, the results of [37] show increased technical difficulties associated with the much more complicated analytic structure of the diagrams: more unitarity cuts contribute and the cancellation of divergences between the various cuts is a subtle affair. In accordance with general theorems of perturbation theory [38], the calculated rate turns out to be finite everywhere except at the $q\bar{q}$ threshold ($Q^2 = 4M_\infty^2$, M_∞ the quark thermal mass) where there remain integrable (square root and logarithm) singularities. However, this threshold is right where the formation time is the longest, and rescattering effects are expected to be largest. Therefore the two loop analysis [37] is not reliable here.

The object of this paper is to compute the imaginary part of the retarded current-current correlator, at momentum Q which is hard ($q^0 \gtrsim T$) but near the light cone ($Q^2 \sim g_s^2T^2$), at leading order in g_s. This current-current correlator is related to the dilepton production rate, per lepton species, via[1] [39]

$$\frac{dN_{\ell^+\ell^-}}{d^4x d^4Q} = \frac{\alpha_{\rm EM}}{12\pi^4 Q^2 (e^{q^0/T}-1)} \, {\rm Im}\, \Pi_{R}{}^{\mu}_{\mu}(Q)\,. \tag{1.1}$$

The calculation requires a resummation of diagrams analogous to that for real photon production. We first review the integral equation already obtained [11] in the case of a real photon ($Q^2 = 0$). Then we extend it to off shell photons. Besides minor kinematic changes to the treatment of [11], this also requires inclusion of longitudinally polarized virtual photons. It is then shown how to obtain an ordinary differential equation by going to impact parameter space, where the equation is solved numerically. The result is more complete, and in some ways simpler, than the two loop perturbative one. We find that multiple scattering effects completely remove the $q\bar{q}$ threshold behavior found in the perturbative treatment; the dilepton spectrum is nonsingular and smooth. Finally, we discuss some phenomenological applications.

2. LPM corrections for longitudinal photons

2.1 Dominant diagrams

In this section, we leave aside the production of photons by Compton scattering ($gq \to \gamma q$) and annihilation ($q\bar{q} \to \gamma g$) which appear at one loop in the perturbative expansion of the HTL effective theory [35, 36] and we consider only the processes of type $qi \to \gamma qi$ and $q\bar{q}i \to \gamma i$ where i denotes a quark, an antiquark or a gluon. These appear at the two-loop level but because of a strong collinear enhancement, powers of $T^2/M_\infty^2 \sim 1/g_{\rm s}^2$ are generated so that they contribute at the leading order in the strong coupling. Higher order diagrams with a ladder topology (see the figure 1) involve the same enhancement mechanism [each new rung in the ladder brings a factor of $\mathcal{O}(g_{\rm s}^2/g_{\rm s}^2)$] and therefore they also contribute at leading order.

The enhancement for ladder diagrams comes from the fact that, in ladder diagrams, the momentum difference between the upper quark and lower quark in each loop of the ladder, which equals the photon momentum, is lightlike, which allows the quark propagators to be simultaneously almost on-shell, leading to a $1/g_{\rm s}^2$ enhancement which cancels the $g_{\rm s}^2$

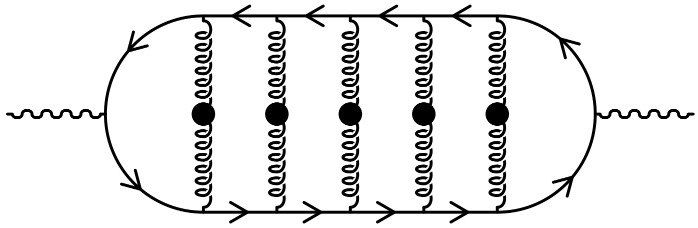

Figure 1: Typical diagram which must be resummed to determine ${\rm Im}\,\Pi^{\mu}_{\mu}$. The gluon lines are soft and HTL-resummed, the solid (quark) lines are hard, approximately on-shell, and resummed to include the dominant imaginary part.

[1] At leading order in $\alpha_{\rm EM}$ and neglecting the lepton mass.

JHEP12(2002)006

from the loop. Non-ladder topologies have more loops than $1/g_s^2$ enhancements, and so are sub-dominant (see [11, 12, 13] for more details[2]). Note also that the quark propagators in the outer loop of figure 1 must be dressed by a thermal width Γ, which is generated by the summation of self-energy corrections involving the HTL gluon propagator.

Finally, when one takes the imaginary part of the photon polarization tensor, some of the gluon propagators (either the ones that appear explicitly in figure 1, or the ones implicitly resummed on the quark propagators) are cut. The particles (quarks and gluons) running in the HTL gluon self-energy are then put on shell, and they correspond to the scattering centers off which the quark scatters.

The summation of these dominant diagrams leads to an integral equation which we now discuss [11, 12, 13].

2.2 Reminder: transverse modes

In [11, 12, 13], Arnold, Moore, and Yaffe summed the set of diagrams of the form shown in figure 1, for lightlike external momentum Q. The lightlike condition allowed them to consider only the two transverse polarizations; in general $\Pi^{\mu\nu}$ has contributions from three polarizations (not four, because $Q_\mu \Pi^{\mu\nu} = 0$), but when $Q^2 = 0$ the longitudinal polarization also vanishes. In terms of the retarded photon polarization tensor, we can rewrite the result presented in these papers as follows:

$$\sum_{i=1,2} \mathrm{Im}\, \Pi_{\mathrm{R}}{}_i^i(Q) \approx \frac{e^2 N_c}{8\pi} \int_{-\infty}^{+\infty} dp_0 \, [n_F(r_0) - n_F(p_0)] \frac{p_0^2 + r_0^2}{(p_0 r_0)^2} \times \\ \times \mathrm{Re} \int \frac{d^2\boldsymbol{p}_\perp}{(2\pi)^2} \, 2\boldsymbol{p}_\perp \cdot \boldsymbol{f}(\boldsymbol{p}_\perp) \,, \tag{2.1}$$

with $r_0 \equiv p_0 + q_0$, $n_F(p_0) \equiv 1/(\exp(p_0/T) + 1)$ the Fermi-Dirac statistical weight, and where the dimensionless function $\boldsymbol{f}(\boldsymbol{p}_\perp)$ obeys the following integral equation:

$$2\boldsymbol{p}_\perp = i\delta E \boldsymbol{f}(\boldsymbol{p}_\perp) + g_s^2 C_F T \int \frac{d^2\boldsymbol{l}_\perp}{(2\pi)^2} \, \mathcal{C}(\boldsymbol{l}_\perp) \, [\boldsymbol{f}(\boldsymbol{p}_\perp) - \boldsymbol{f}(\boldsymbol{p}_\perp + \boldsymbol{l}_\perp)] \,. \tag{2.2}$$

In this integral equation, $\delta E \equiv q_0(\boldsymbol{p}_\perp^2 + M_\infty^2)/(2p_0 r_0)$ is an energy denominator arising from nearly on-shell quark propagators; it can be interpreted as the inverse formation time of the photon. Here $M_\infty^2 \equiv g_s^2 C_F T^2/4$ is the thermal mass of a hard quark at leading order (or equivalently, in the HTL approximation). $C_F = (N_c^2 - 1)/2N_c$ is the Casimir in the fundamental representation of the gauge group $\mathrm{SU}(N_c)$; in QCD it is 4/3. The second term arises from the gluon exchange lines in figure 1 (both those shown and those hidden in the fact that the quark line self-energies are resummed). The factor $\mathcal{C}(\boldsymbol{l}_\perp)$ is the kernel of a collision integral describing an elementary collision of the emitter with another particle of the plasma. In terms of the transverse and longitudinal HTL self-energies $\Pi_{T,L}(l_0/l)$ of the

[2] In particular, there is a subtlety regarding "crossed rungs," which by the above argument should be leading but which are not, because the poles of the two near-shell propagators fail to pinch the frequency contour.

exchanged gluon, it is given by [11, 12, 13]:

$$\mathcal{C}(\boldsymbol{l}_\perp) \equiv \int \frac{dl_0 dl_z}{(2\pi)^2} 2\pi\delta(l_0 - l_z)\,\frac{1}{l_0} \times$$
$$\times \sum_{\alpha=L,T} \frac{2\,\mathrm{Im}\,\Pi_\alpha(L)}{(L^2 - \mathrm{Re}\,\Pi_\alpha(L))^2 + (\mathrm{Im}\,\Pi_\alpha(L))^2}\, P_\alpha^{\mu\nu}(L)\widehat{Q}_\mu\widehat{Q}_\nu\,, \tag{2.3}$$

with $\widehat{Q}_\mu \equiv (1, \boldsymbol{q}/q)$ and $P^{\mu\nu}_{T,L}(L)$ the transverse or longitudinal projector for a gluon of momentum L. In [8], it was shown that this collision kernel can in fact be calculated exactly thanks to a sum rule satisfied by the HTL gluon propagator, leading to a very simple expression:

$$\mathcal{C}(\boldsymbol{l}_\perp) = \frac{1}{\boldsymbol{l}_\perp^2} - \frac{1}{\boldsymbol{l}_\perp^2 + m_{\mathrm{D}}^2}\,, \tag{2.4}$$

where $m_{\mathrm{D}}^2 \equiv g_{\mathrm{s}}^2 T^2 [N_{\mathrm{c}} + N_{\mathrm{F}}/2]/3$ is the Debye mass in an $\mathrm{SU}(N_{\mathrm{c}})$ gauge theory with N_{F} fundamental representation flavors.

Generalizing the above equations to the case of the transverse modes of a massive photon is straightforward, as one needs only to replace M_∞^2 in δE by the following combination of the quark mass and the photon invariant mass [4, 12]:[3]

$$M_\infty^2 \to M_{\mathrm{eff}}^2 \equiv M_\infty^2 + \frac{Q^2}{q_0^2} p_0 r_0\,. \tag{2.6}$$

For $Q^2 > 4M_\infty^2$, this quantity can become negative and δE can vanish. In this case, M_{eff}^2 should be understood as having an infinitesimal imaginary part $ip_0 r_0 \epsilon/q_0$, as one can readily see from its derivation from the quark energy denominators.

This is not enough to fully calculate the dilepton production rate; one must also include the longitudinal mode of the off shell (virtual) photon. We calculate the contribution of this mode in the next subsection.

2.3 Longitudinal mode

The contribution of the longitudinal mode can be derived simply by following a procedure similar to the one employed in [11, 12]. Let us start by writing:[4]

$$\Pi_{\mathrm{L}}(Q) \equiv \epsilon_{\mathrm{L}}^\mu(Q)\epsilon_{\mathrm{L}}^{\nu *}(Q)\Pi_{\mu\nu}(Q)\,, \tag{2.7}$$

[3]This substitution is sufficient as long as we are considering hard photons that are not too virtual. It can be used if the following inequality is satisfied:

$$Q^2 \ll q_0^2\,. \tag{2.5}$$

If this is not the case, then the kinematics is no longer dominated by small angle scatterings and all of the above equations must be reconsidered. Note that this inequality implies that one can interchange q_0 and the 3-momentum q at leading order, in all quantities where no cancellation $(q_0 - q)$ occurs.

[4]Note that, since the sum over polarizations $\sum_\lambda \epsilon_\lambda^\mu(Q)\epsilon_\lambda^{*\nu}(Q)$ can be replaced by $-g^{\mu\nu}$ thanks to Ward identities, it is the *opposite* of Π_{L} that must be added to $\Pi_i{}^i$ in order to obtain the full $\Pi_\mu{}^\mu$.

with the following longitudinal polarization vector

$$\epsilon^{\mu}_{\rm L}(Q) \equiv \frac{(q,0,0,q_0)}{\sqrt{Q^2}}\,. \tag{2.8}$$

Making use of the Ward identity $Q^\mu \Pi_{\mu\nu}(Q) = 0$ satisfied by the photon polarization tensor, we obtain

$$\Pi_{\rm L}(Q) = \frac{Q^2}{q^2}\Pi^{00}(Q)\,. \tag{2.9}$$

Therefore, we see that we need only the 00 component of the photon polarization tensor.[5] This also makes clear why $\Pi_{\rm L} = 0$ for real photons.

Now we must evaluate $\Pi^{00}(Q)$ summing over all diagrams of the type shown in figure 1. Recall that the retarded/advanced HTL propagator of a hard quark can be approximated by:

$$S_{R,A}(P) \approx i\frac{\overline{\not P}}{\overline{P}^2 \pm ip_0\epsilon}\,, \tag{2.10}$$

where $\overline{P} \equiv (p_0, \sqrt{\boldsymbol{p}^2 + M_\infty^2}\hat{\boldsymbol{p}})$. It is easy to verify that one can replace the Dirac matrix $\overline{\not P}$ in the numerator of the effective quark propagator by:

$$\overline{\not P} \to \epsilon(p_0)\; w(\epsilon(p_0)\,\boldsymbol{p})\overline{w}(\epsilon(p_0)\,\boldsymbol{p})\,, \tag{2.11}$$

where we denote $\epsilon(p_0)$ the sign of p_0, and $w(\boldsymbol{p}) \equiv \sqrt{\omega_p/p}\,u(\boldsymbol{p})$ with $u(\boldsymbol{p})$ the usual massless[6] spinor normalized according to $u(\boldsymbol{p})\overline{u}(\boldsymbol{p}) = \not P$ (implicitly, $p_0 > 0$ in this relation) and $\omega_p \equiv \sqrt{\boldsymbol{p}^2 + M_\infty^2}$. Then, one can associate the spinors w and $\overline{w}$ in the numerator of the propagator with the vertices,

$$\gamma^\sigma \to \underline{\gamma}^\sigma \equiv \overline{w}(\epsilon(p_0+l_0)(\boldsymbol{p}+\boldsymbol{l}))\gamma^\sigma w(\epsilon(p_0)\boldsymbol{p})\,, \tag{2.12}$$

if $L \equiv (l_0, \boldsymbol{l})$ is the momentum of the gauge boson entering in the vertex. For the vertices coupling the quark loop to the soft gluons, we can simply neglect the gluon momentum, and write $\underline{\gamma}^\sigma \approx 2P^\sigma_\epsilon$ with $P_\epsilon \equiv (p_0, \epsilon(p_0)\boldsymbol{p})$. It is slightly more complicated to deal with the $\gamma q\bar{q}$ vertices since the photon can be hard, but we need only the 0 component $\underline{\gamma}^0$, in the configuration where the quark and the photon are nearly collinear. In this limit, we find: $\underline{\gamma}^0 \approx 2\sqrt{pr} \approx 2\sqrt{|p_0 r_0|}$.

Now that all the spinor structure has been absorbed in the vertices, performing the Dirac's trace is trivial; $\mathrm{Tr}(\boldsymbol{1}) = 4$. In fact, the vertices coupling the quark loop to the gluons are the same as in a scalar theory, and the only differences between scalar and fermionic particles lie in the coupling to the photon and in the statistical weights. Therefore, we can

[5] To be consistent, if HTL fermion propagators are necessary then HTL corrections to the $q\bar{q}\gamma$ vertices are also needed [37]. However, the complete effect of this vertex is to ensure that the Ward identity is satisfied, by rescaling Π_{zz} by an $O(g_s^2)$ amount with respect to Π_{00}. By using the Ward identity to express $\Pi_{\rm L}$ in terms of Π_{00}, we have taken this into account, and can compute Π_{00} at leading order only.

[6] This property is true because the HTL resummation preserves the chiral invariance of the bare theory.

mimic[7] eq. (2.1) for the retarded self-energy of the longitudinal photon in order to obtain

$$\mathrm{Im}\,\Pi_{\mathrm{L}}(Q) = -\frac{e^2N_c}{4\pi}\frac{Q^2}{q^2}\int_{-\infty}^{+\infty} dp_0[n_{_F}(r_0)-n_{_F}(p_0)]\frac{\epsilon(p_0r_0)}{p_0r_0} \times \mathrm{Re}\int \frac{d^2\boldsymbol{p}_\perp}{(2\pi)^2}2\sqrt{|p_0r_0|}\,g(\boldsymbol{p}_\perp)\,, \tag{2.13}$$

where $g(\boldsymbol{p}_\perp)$ is a dimensionless scalar function which describes the resummed coupling of the quark to the longitudinal photon, and obeys the following integral equation, in complete analogy[8] with eq. (2.2),

$$2\sqrt{|p_0r_0|} = i\delta E g(\boldsymbol{p}_\perp) + g_s^2C_F T\int \frac{d^2\boldsymbol{l}_\perp}{(2\pi)^2}\mathcal{C}(\boldsymbol{l}_\perp)[g(\boldsymbol{p}_\perp)-g(\boldsymbol{p}_\perp+\boldsymbol{l}_\perp)]\,. \tag{2.14}$$

Combining the result of [11] and the above formulas for the longitudinal mode, we can write the equation for the complete polarization tensor of a massive photon:

$$\mathrm{Im}\,\Pi_{\mathrm{R}\,\mu}^{\ \mu}(Q) \approx \frac{e^2N_c}{2\pi}\int_{-\infty}^{+\infty} dp_0\,[n_{_F}(r_0)-n_{_F}(p_0)]\times \times\mathrm{Re}\int\frac{d^2\boldsymbol{p}_\perp}{(2\pi)^2}\left[\frac{p_0^2+r_0^2}{2(p_0r_0)^2}\boldsymbol{p}_\perp\cdot\boldsymbol{f}(\boldsymbol{p}_\perp)+\frac{1}{\sqrt{|p_0r_0|}}\frac{Q^2}{q^2}g(\boldsymbol{p}_\perp)\right], \tag{2.15}$$

where $\boldsymbol{f}(\boldsymbol{p}_\perp)$ and $g(\boldsymbol{p}_\perp)$ respectively obey eq. (2.2) and eq. (2.14). Note that this expression is valid for one flavor of the emitting quark, with electrical charge e (but N_F flavors of quarks are taken into account for the scattering centers, as can be seen from the expression of the Debye mass). For the emission by N_F families of quarks with electrical charges e_s, one must substitute:

$$e^2 \to \sum_{f=1}^{N_F} e_f^2\,. \tag{2.16}$$

2.4 Born term

Before solving numerically the above integral equations, it is interesting to show that they contain the contribution of the Born term, corresponding to the direct $q\bar{q}$ annihilation into a virtual photon. Indeed, if we solve the equations (2.2) and (2.14) at order 0 in the collision term, we obtain respectively

$$\boldsymbol{p}_\perp\cdot\boldsymbol{f}(\boldsymbol{p}_\perp) = -4\boldsymbol{p}_\perp^2\frac{p_0r_0}{q_0}\frac{i}{\boldsymbol{p}_\perp^2+M_{\text{eff}}^2+i\frac{p_0r_0}{q_0}\epsilon} \tag{2.17}$$

[7] The substitution rules are the following: there is a $-$ sign since it is the opposite of Π_{L} that enters in $\Pi_\mu{}^\mu$. A factor $\epsilon(p_0r_0)$ comes from the last loop (other factors of $\epsilon(p_0r_0)$ are kept inside the function $g(\boldsymbol{p}_\perp)$). The factor Q^2/q^2 comes from the relationship between Π_{L} and Π_{00}, and the factor $(p_0^2+r_0^2)/(p_0r_0)$ must be removed from eq. (2.1) since it was there to account for the coupling of the quark to the transverse modes of the photon.

[8] Just replace the "tree-level" vertex $2\boldsymbol{p}_\perp$ (i.e. the starting point of the iteration) by $2\sqrt{|p_0r_0|}$ and the function $\boldsymbol{f}(\boldsymbol{p}_\perp)$ by $g(\boldsymbol{p}_\perp)$.

JHEP12(2002)006

and

$$g(\boldsymbol{p}_\perp) = -4\sqrt{|p_0 r_0|}\frac{p_0 r_0}{q_0}\frac{i}{\boldsymbol{p}_\perp^2 + M_{\rm eff}^2 + i\frac{p_0 r_0}{q_0}\epsilon}\,. \tag{2.18}$$

These quantities yield a nonzero real part, when integrated over $\boldsymbol{p}$, provided that $M_{\rm eff}^2 < 0$. This occurs when $Q^2 > 4M_\infty^2$, i.e. above the threshold for the process $q\bar{q} \to \gamma^*$. Keeping only the real part and substituting these values in eq. (2.15), we get

$$\mathrm{Im}\,\Pi_{\mathrm{R}\,\mu}^{\;\mu}(Q) = \frac{e^2 N_{\rm c}}{2\pi}\int_{-\infty}^{+\infty} dp_0\, \theta(-M_{\rm eff}^2)[n_{_F}(r_0) - n_{_F}(p_0)]\left[Q^2 + M_\infty^2\frac{p_0^2 + r_0^2}{r_0 p_0}\right], \tag{2.19}$$

which is identical to the expression obtained in [37] for the Born contribution to the virtual photon retarded self-energy.[9]

Therefore, the only leading order terms that are not included in eq. (2.15) are the $2 \to 2$ processes considered in [35, 36]. This extra contribution should be added to our results in order to obtain the complete leading order dilepton spectrum.

3. Formulation in impact parameter space

It is possible to approach the integral equations analytically by two approximative methods. The first is to treat the collision term $\mathcal{C}$ as small, and solve the integral equation iteratively in this quantity. The leading $\mathcal{C} = 0$ result is the Born term given above; the next order, from substituting eq. (2.17), (2.18) into the collision term, gives the results of Aurenche et al. [37]. This approach converges well at large Q^2. Alternatively, one may take δE to be small and work to leading logarithmic order in this limit. This approach should work very close to the Born threshold. Neither approach works in all kinematic regimes, and in general it is necessary to treat the integral equation numerically. This has been done for on-shell photon production, in momentum space, by using a variational approach [12, 40].

However, a simpler method can be obtained after going to impact parameter space by a Fourier transform. Doing so is made practical by the fact that the collision term is known in closed form and has a rather simple Fourier transform. The method was outlined in [8] in the case of real photon production, and can be extended to the case of dileptons.

Let us first introduce the Fourier transforms:

$$\begin{aligned} \boldsymbol{f}(\boldsymbol{p}_\perp) &\equiv \int d^2\boldsymbol{b}\, e^{-i\boldsymbol{p}_\perp\cdot\boldsymbol{b}}\, \boldsymbol{f}(\boldsymbol{b})\,, \\ g(\boldsymbol{p}_\perp) &\equiv \int d^2\boldsymbol{b}\, e^{-i\boldsymbol{p}_\perp\cdot\boldsymbol{b}}\, g(\boldsymbol{b})\,, \end{aligned} \tag{3.1}$$

where we use the same letter to denote both a function and its Fourier transform, as the argument should make obvious which one enters in a particular expression. The functions

[9] This expression does not look like the naive Born term; in particular it has an extra piece proportional to M_∞^2. This is because it is computed within HTL resummed perturbation theory. The fermionic propagators are shifted in a way which gives them massive dispersion relations without violating chiral symmetry, and there is a corresponding correction to the vertex (as dictated by the Ward identity). The dependence on M_∞^2 arises from these two effects. For more details see [37].

$\boldsymbol{f}(\boldsymbol{b})$ and $g(\boldsymbol{b})$ obey simple partial differential equations:

$$\begin{aligned} i\frac{q_0}{2p_0r_0}(M_{\rm eff}^2-\Delta_\perp)\boldsymbol{f}(\boldsymbol{b})+g_{\rm s}^2C_{\rm F}TD(m_{\rm D}b)\boldsymbol{f}(\boldsymbol{b}) &= -2i\nabla_\perp\delta(\boldsymbol{b})\,,\\ i\frac{q_0}{2p_0r_0}(M_{\rm eff}^2-\Delta_\perp)g(\boldsymbol{b})+g_{\rm s}^2C_{\rm F}TD(m_{\rm D}b)g(\boldsymbol{b}) &= 2\sqrt{|p_0r_0|}\delta(\boldsymbol{b})\,, \end{aligned} \tag{3.2}$$

where we denote

$$D(m_{\rm D}b)\equiv\frac{1}{2\pi}\left[\gamma_{\rm E}+\ln\left(\frac{m_{\rm D}b}{2}\right)+K_0(m_{\rm D}b)\right], \tag{3.3}$$

with K_0 the modified Bessel function of the second kind and $\gamma_{\rm E}$ the Euler constant, $\gamma_{\rm E}\approx 0.577$. As we shall see later, the inhomogeneous terms proportional to $\delta(\boldsymbol{b})$ in these equations determine uniquely the normalization of the solution by imposing the small b behavior of the solution. The quantities that are needed in eq. (2.15) in order to compute the photon polarization tensor are then given by

$$\begin{aligned} {\rm Re}\int\frac{d^2\boldsymbol{p}_\perp}{(2\pi)^2}\boldsymbol{p}_\perp\cdot\boldsymbol{f}(\boldsymbol{p}_\perp) &= \lim_{b\to 0^+}{\rm Im}\,\nabla_\perp\cdot\boldsymbol{f}(\boldsymbol{b})\,,\\ {\rm Re}\int\frac{d^2\boldsymbol{p}_\perp}{(2\pi)^2}g(\boldsymbol{p}_\perp) &= \lim_{b\to 0^+}{\rm Re}\,g(\boldsymbol{b})\,. \end{aligned} \tag{3.4}$$

We must now determine the boundary conditions to impose on the solutions of eqs. (3.2) in order to determine them uniquely. First, the functions $\boldsymbol{f}(\boldsymbol{b})$ and $g(\boldsymbol{b})$ must remain bounded when $|\boldsymbol{b}|\to+\infty$. The most general large b behavior is the sum of an exponentially growing and and exponentially shrinking solution; only the shrinking solution is allowed, so the required boundary condition is

$$\begin{aligned} \lim_{b\to+\infty}\boldsymbol{f}(\boldsymbol{b}) &= 0\,,\\ \lim_{b\to+\infty}g(\boldsymbol{b}) &= 0\,. \end{aligned} \tag{3.5}$$

Another boundary condition can be derived at $b=0$, from the small distance behavior of the differential equations satisfied by $\boldsymbol{f}(\boldsymbol{b})$ and $g(\boldsymbol{b})$. It is easy to check that $D(m_{\rm D}b)$ vanishes like $b^2\ln(b)$ when b approaches zero, so that the term proportional to $D(m_{\rm D}b)$ becomes irrelevant in this limit. In fact, the dominant small b behavior is completely determined by the laplacian and the inhomogeneous term. One finds easily:

$$\begin{aligned} \boldsymbol{f}(\boldsymbol{b}) &\underset{b\to 0^+}{\approx} \frac{2}{\pi}\frac{p_0r_0}{q_0}\frac{\widehat{\boldsymbol{b}}}{b}+O(\boldsymbol{b})\,,\\ g(\boldsymbol{b}) &\underset{b\to 0^+}{\approx} \frac{2i}{\pi}\frac{p_0r_0}{q_0}\sqrt{|p_0r_0|}\,\ln(m_{\rm D}b)+O(b^0)\,. \end{aligned} \tag{3.6}$$

Note that even if these small b behaviors are singular, they do not affect eqs. (3.4) since the singular part of $\boldsymbol{f}(\boldsymbol{b})$ is purely real, and the singular part of $g(\boldsymbol{b})$ is purely imaginary. Since the differential equations (3.2) are second order affine equations, a solution is uniquely determined by two boundary conditions. Therefore, eqs. (3.2), (3.4) together with the boundary conditions (3.5) and (3.6) provide a complete reformulation of the original problem.

JHEP12(2002)006

These differential equations can be simplified further by noting that rotational invariance in the transverse plane implies that $g(\boldsymbol{b})$ depends only on the modulus b, and that $\boldsymbol{f}(\boldsymbol{b})$ can be written as $\boldsymbol{f}(\boldsymbol{b}) \equiv \boldsymbol{b} h(b)$. Therefore, we have

$$\begin{aligned} \Delta_\perp \boldsymbol{f}(\boldsymbol{b}) &= \boldsymbol{b}\left[h''(b) + 3\frac{h'(b)}{b}\right], \\ \Delta_\perp g(\boldsymbol{b}) &= g''(b) + \frac{g'(b)}{b}. \end{aligned} \tag{3.7}$$

In terms of the new function $h(b)$, the first of eqs. (3.4) becomes

$$\mathrm{Re}\int \frac{d^2\boldsymbol{p}_\perp}{(2\pi)^2}\boldsymbol{p}_\perp \cdot \boldsymbol{f}(\boldsymbol{p}_\perp) = 2\lim_{b\to 0^+} \mathrm{Im}\, h(b)\,, \tag{3.8}$$

and the desired differential equation is

$$i\frac{q_0}{2p_0 r_0}\left(M_{\mathrm{eff}}^2 - \partial_b^2 - 3\frac{\partial_b}{b}\right)h(b) + g_{\mathrm{s}}^2 C_{\mathrm{F}} T D(m_{\mathrm{D}} b) h(b) = 0\,, \tag{3.9}$$

with boundary condition

$$h(b) \underset{b\to 0^+}{\approx} \frac{2p_0 r_0}{\pi q_0 b^2} + O(1)\,. \tag{3.10}$$

4. Numerical resolution

General nonlinear ordinary differential equations with mixed boundary conditions are usually solved with the "overshoot-undershoot" method. However, because our differential equations are linear, they can be solved by a single application of a quadratures ODE solver (specific algorithms can be found in [41]). We will describe the procedure for $h(b)$; the procedure for $g(b)$ is completely analogous.[10]

What we want is the imaginary part, at the origin, of the exponentially decaying solution of eq. (3.9), normalized to satisfy the boundary condition at zero, eq. (3.10). This can be achieved by finding the decaying solution, with arbitrary normalization, and scaling it to have the desired small b behavior (including rotation by a complex phase to make the $1/b^2$ piece purely real). To find the pure decaying solution, it is sufficient to begin at large b with arbitrary (nonzero) initial data for $h(b)$ and $h'(b)$ and to evolve the differential equation inwards towards $b = 0$. The solution which grows exponentially at large b shrinks as we evolve towards the origin, the normalizable solution grows.

To determine what value of b is sufficient to suppress the wrong solution by a suitably large factor, we can determine the approximate large b behavior of eq. (3.9) by approximating D to be constant (at large b it only varies logarithmically, $D(m_{\mathrm{D}}b) \simeq (\gamma_{\mathrm{E}} + \log(m_{\mathrm{D}}b/2))$) and dropping the $3\partial_b/b$ term. The result is,

$$h\left(b \gg \frac{1}{m_{\mathrm{D}}}\right) \sim c_+ e^{\lambda_+ m_{\mathrm{D}} b} + c_- e^{\lambda_- m_{\mathrm{D}} b}\,,$$

[10]The procedure described in the present paper is slightly different from the one outlined in [8]. The latter has also been checked to work, albeit more slowly since it requires two runs of the ODE solver instead of one.

$$\lambda_{\pm} = \pm\sqrt{M_{\rm eff}^2 - i\frac{2g_{\rm s}^2 C_{\rm F} T p_0 r_0}{q_0} D(m_{\rm D} b)}\,. \tag{4.1}$$

We should choose initial data at a value of b, large enough that the ratio of exponentials $e^{\lambda_+ m_{\rm D} b}/e^{\lambda_- m_{\rm D} b}$ is abundantly larger than the desired accuracy. It is also easy to use the above equations to ensure the initial data for h and h' are almost those of the shrinking solution, so the coefficient c_+ is initialized close to zero. (This procedure is not exact because of the $3\partial_b/b$ term we dropped, and the b dependence of D which we neglected.) Starting with this initial data, the ODE, eq. (3.9), is evolved towards $b = 0$ by standard methods, and the coefficients of the b^{-2} and b^0 behavior are extracted.

For the extraction of the b^{-2} and b^0 behavior, it is helpful to determine the small b behavior a little more precisely. At small b, $D(m_{\rm D} b) \sim b^2 \ln(1/m_{\rm D} b)$ is negligible; but the $M_{\rm eff}^2$ term may be large enough, only to be negligible at quite small b, where numerical error in the b^{-2} term can pollute the b^0 term. Hence it is useful to match to the behavior neglecting the $D(m_{\rm D} b)$ term but including all other terms;

$$h\left(b \ll \frac{1}{m_{\rm D}}\right) \sim c_1 \frac{M_{\rm eff} K_1(M_{\rm eff} b)}{b} + c_2 \frac{I_1(M_{\rm eff} b)}{M_{\rm eff} b}\,, \tag{4.2}$$

with I_1 and K_1 the modified Bessel functions of the first and second kind (for $M_{\rm eff}^2 < 0$ one should replace K, I with Y, J and $M_{\rm eff}$ with $|M_{\rm eff}|$). The desired quantity, eq. (3.8), is just $(4p_0 r_0/\pi q_0)\,{\rm Im}\, c_2/c_1$. (By working in terms of c_2/c_1, we avoid needing to rescale the solution to the appropriate normalization.) It is also possible to include the small effect of $D(m_{\rm D} b)$ perturbatively.

The treatment of $g(h)$ is completely analogous; the asymptotic large b analysis is the same. The differential equation differs only in that the coefficient of the ∂_b/b term is 1 instead of 3, so the small b behavior is

$$g\left(b \ll \frac{1}{m_{\rm D}}\right) \sim c_1 K_0(M_{\rm eff} b) + c_2 I_0(M_{\rm eff} b)\,, \tag{4.3}$$

and the desired quantity, eq. (3.4), is $(2p_0 r_0 \sqrt{p_0 r_0}/\pi q_0)\,{\rm Im}\, c_2/c_1$.

5. Phenomenology

The major problem in the 2-loop evaluation of the dilepton rate was the presence of a singularity at the location of the tree-level threshold $Q^2 = 4M_\infty^2$. Basically, this divergence is a common feature of any fixed loop order calculation near a phase-space boundary. A first point to check in the present resummation is that this problem has been cured. This is readily seen in the plot of figure 2. In this plot, 'single scattering' denotes the contribution calculated in [37], which is the term of order $\mathcal{C}^1$ in an iterative small $\mathcal{C}$ expansion of the integral equations (2.2) and (2.14) (the starting point of the iteration being the terms of order $\mathcal{C}^0$ derived in eqs. (2.17) and (2.18)). One can see that including all orders in $\mathcal{C}(\boldsymbol{l}_\perp)$ makes the result continuous at $Q^2 = 4M_\infty^2$. Note that the Born term (i.e. the contribution of $\mathcal{C}^0$ in the iterative solution of the integral equations) is not included in this plot.

JHEP12(2002)006

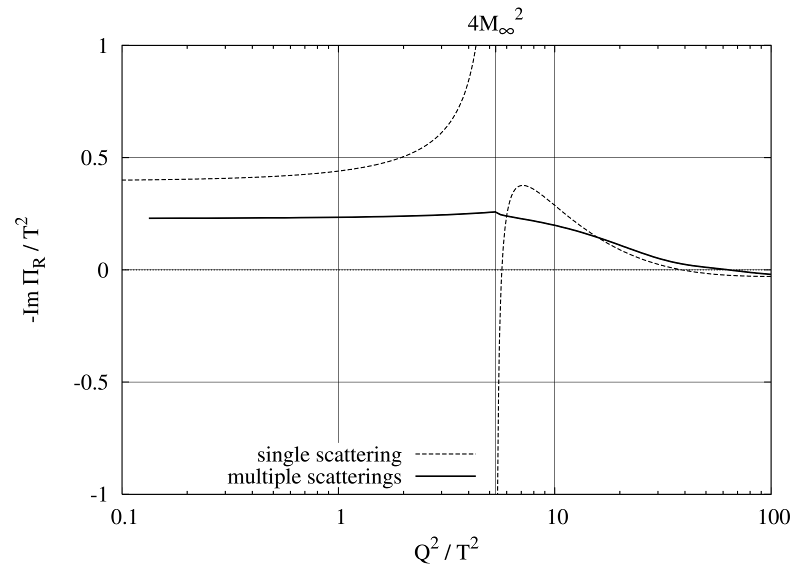

Figure 2: The sum of all the multiple scattering diagrams compared to the single scattering contribution only. In this plot $\alpha_s = 0.3$ and $q_0/T = 50$.

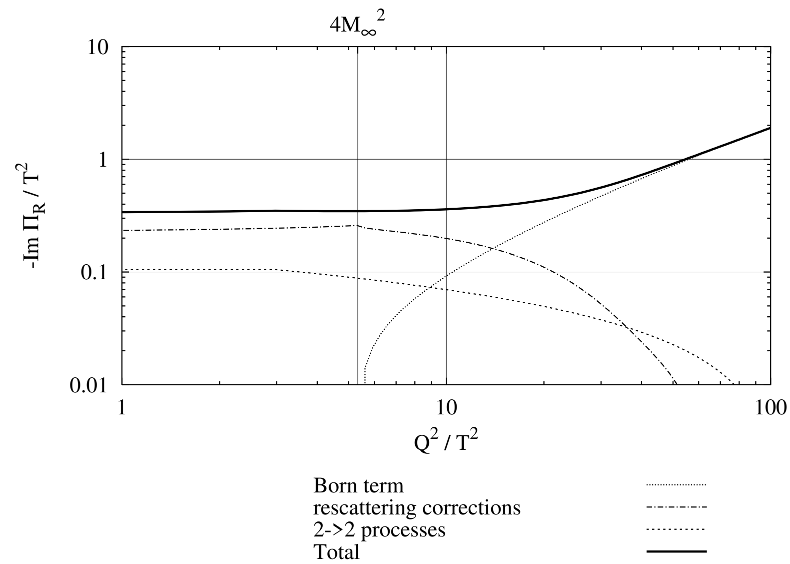

Figure 3: All the contributions to $\mathrm{Im}\,\Pi_R$ up to $\mathcal{O}(\alpha_s)$. In this plot $\alpha_s = 0.3$ and $q_0/T = 50$.

If one now includes also the Born term, an interesting feature of the result is that there is no trace of the threshold at $Q^2 = 4M_\infty^2$. In other words, the step function $\theta(Q^2 - 4M_\infty^2)$ behavior which is characteristic of the Drell-Yan process $q\bar{q} \to \gamma^* \to l^+l^-$ is completely washed out when one corrects this process by in-medium rescatterings. This is illustrated in figure 3. This property is easy to understand after the integral equations (2.2) and (2.14), whose solution contains the Born term and all the rescattering corrections, have been rewritten as differential equations with mixed boundary conditions. The parameter Q^2 enters only as a coefficient in the linear differential equations (3.2). Because of the term containing D, the solution is always regular and exponentially falling at large b (see

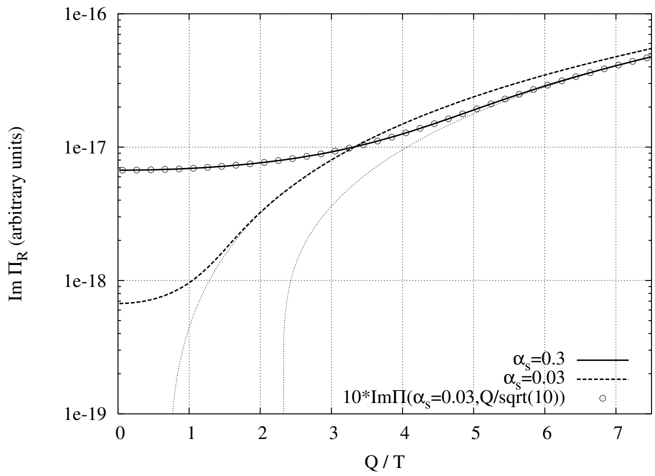

Figure 4: $\mathrm{Im}\,\Pi_R$ as a function of the photon invariant mass for two values of the strong coupling constant. The dotted lines are the corresponding Born terms. The circles illustrate the scaling law of eq. (5.1). The value of q_0/T is set to 30 in this plot.

eq. (4.1)). This ensures that it evolves smoothly as Q^2 changes.[11] In figure 3 and following, the contribution of the $2 \to 2$ processes is taken from [35][12]

One can also add that the smoothing of the threshold depends on the value of the strong coupling constant g_s, as illustrated in figure 4. On this plot, one can see a remnant of the threshold at small coupling, while it completely disappears at strong coupling. We also illustrate on this plot a simple scaling property of the function $\mathrm{Im}\,\Pi_{R\,\mu}^{\;\mu}(\alpha_s, q_0, Q^2, T)$; from equations (2.15), (2.2) and (2.14) one can show that the dependence on α_s scales according to

$$\mathrm{Im}\,\Pi_{R\,\mu}^{\;\mu}(\alpha_s, q_0, Q^2, T) = \alpha_s T^2 F\left(\frac{q_0}{T}, \frac{Q^2}{\alpha_s T^2}\right), \tag{5.1}$$

where F is a dimensionless function of q_0/T and $Q^2/\alpha_s T^2$ (in other words, gT is the natural unit for the photon invariant mass in this problem).

Concerning the respective size of the transverse and longitudinal photon polarizations, we have checked that at low Q^2/q_0^2, the rate is, as expected, dominated by the transverse mode and that the longitudinal mode becomes important only when Q^2/q_0^2 approaches 1, a region where rescattering effects are not very large.

[11] An equivalent explanation, in momentum space, for the smoothness at threshold is the following: in eqs. (2.2) and (2.14) respectively, the $\boldsymbol{f}(\boldsymbol{p}_\perp)$ and $g(\boldsymbol{p}_\perp)$ terms under the integral originate from the damping rate of the fermion (due to the rescattering of the fermion in the medium) and, very roughly, provide an imaginary part to δE. The pole occurring at $Q^2 > 4M_{\mathrm{eff}}^2$ in the Born term is then shifted away from the real axis by an amount proportional to the damping rate and no $\theta(-M_{\mathrm{eff}}^2)$ appears.

[12] One caveat should be mentioned here: the result of [35] cannot be extrapolated to the limit of vanishing photon invariant mass, because it was derived under the assumption that the nonzero photon mass would play the role of the infrared cutoff. Therefore, when at small Q^2 the photon polarization tensor of [35] becomes larger than the real photon polarization tensor of [2], we consider that the zero photon mass limit is reached and we use the result of [2]. This is an imperfect approximation, reflecting a gap in the current literature.

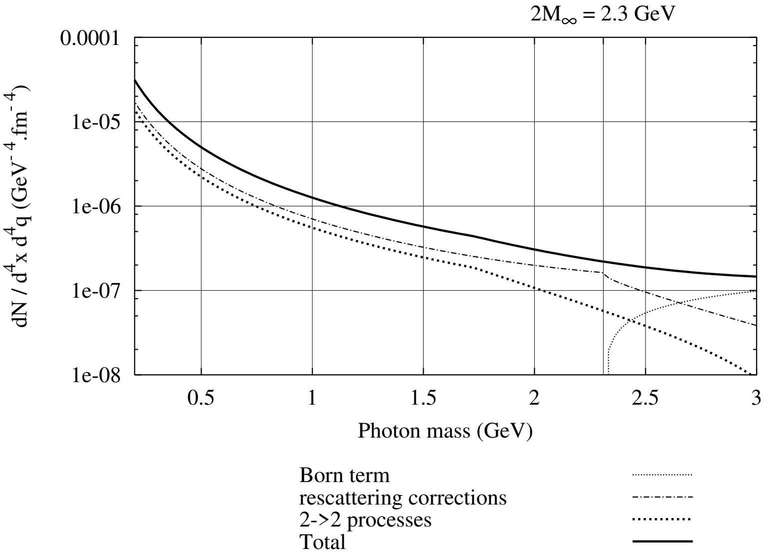

Figure 5: Dependence of the dilepton rate on the mass of the pair. In this plot $T = 1\,\mathrm{GeV}$, $q_0 = 5\,\mathrm{GeV}$, $N_F = 2$ and $\alpha_s = 0.3$.

In order to illustrate how the LPM corrections evaluated in the present paper affect the dilepton production rate, we present now a series of plots for realistic values of the parameters. We emphasize first, though, that our approach only computes the dilepton emission at leading order in g_s, and that for realistic values of $\alpha_s \sim 1/3$ the perturbative series probably shows poor convergence and our results should perhaps be interpreted as factor of 2 estimates.

Figure 5 shows the dependence of the dilepton rate with respect to the mass of the lepton pair, the pair total energy being set to $5\,\mathrm{GeV}$, for a temperature of $1\,\mathrm{GeV}$ (we consider 2 quark flavors, and take $\alpha_s = 0.3$). One can see on this plot that considering only the Born term and the $2 \to 2$ processes is not a good approximation. In the low mass region ($Q \leq 1\,\mathrm{GeV}$), the rescattering diagrams more than double the contribution of the $2 \to 2$ processes. In the intermediate mass region, near the tree-level threshold, the effect of these processes is even larger and they completely wash out the threshold, as explained before. It is only for large pair masses ($Q \geq 3\,\mathrm{GeV}$) that these corrections start being small compared to the Born term. However, the ratio Q/q_0 of the mass over the energy of the pair becomes large and the approximations used cease to be reliable.

One can also study how this mass dependence varies with the temperature. In figure 6, we display the total dilepton rate for two different temperatures ($T = 1\,\mathrm{GeV}$ and $T = 500\,\mathrm{MeV}$), the other parameters being the same as in the previous figure. In this plot, the vertical lines indicate how much of the total rate is due to the rescattering contributions. In addition to the drop one expects when one lowers the temperature, it is possible to see that the effect of these processes are limited to smaller values of the mass Q. This is because the scale which controls these effects is controlled by thermal masses proportional to T.

Finally, in figure 7, we display the dilepton rate as a function of the pair energy, the mass Q being fixed. At large energy, one can see the typical exponential drop in

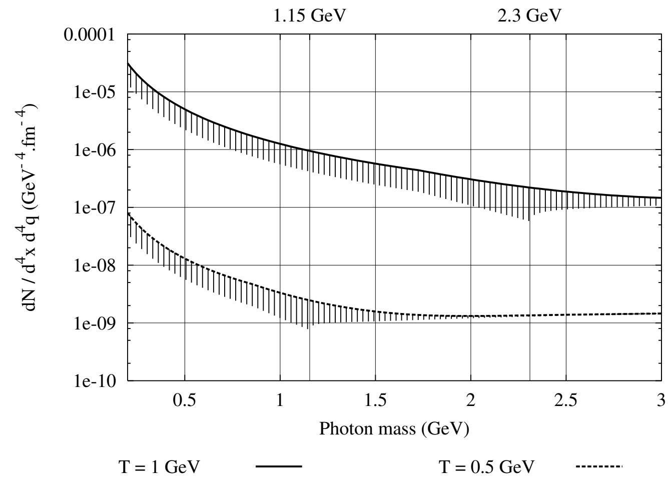

Figure 6: Dependence of the dilepton rate on the temperature. The vertical lines represent the contribution of the processes involving scatterings in the medium. In this plot $q_0 = 5\,\text{GeV}$, $N_{_F} = 2$ and $\alpha_{\rm s} = 0.3$.

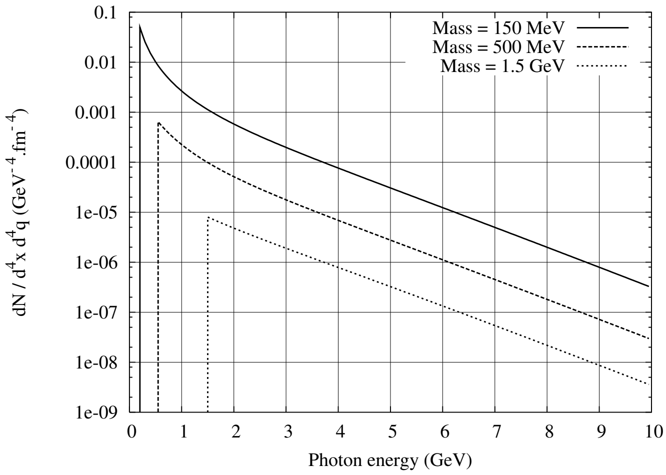

Figure 7: Dilepton rate as a function of the pair energy, for $Q = 150\,\text{MeV}$, $Q = 500\,\text{MeV}$ and $Q = 1.5\,\text{GeV}$. In this plot $T = 1\,\text{GeV}$, $N_{_F} = 2$ and $\alpha_{\rm s} = 0.3$.

$\exp(-q_0/T)$. More precisely, the asymptotic behavior of the dilepton rate at large q_0 and fixed Q is in $\sqrt{q_0}\exp(-q_0/T)$, the factor $\sqrt{q_0}$ being characteristic of the LPM effect at large photon energies. In addition, increasing the pair mass has the expected effect of making the rate decrease. Note that the curves in this plot are unreliable at the low end, near $q_0 \approx Q$, since the approximation $q_0 \approx q$ is certainly invalid in this region. This is the region where the lepton pair is produced almost at rest in the plasma frame ($q \approx 0$), which precludes any use of a collinear kinematics.

6. Conclusions

In this paper we completed the $\mathcal{O}(\alpha_{\rm s})$ calculation of the rate of low-mass lepton pairs produced at large momentum in a plasma in equilibrium. Production of the pairs in multiple scattering processes are found to be important and even dominate the rate in a wide range of masses. An interesting result is the absence of a threshold in the mass dependence of the virtual photon: the rescattering processes completely wash out the $q\bar{q}$ annihilation threshold naively expected. The absence of a threshold in the photon invariant mass looks different from the recent results of lattice calculations [42, 43] where a pronounced threshold is observed in the production of a lepton pair at rest in quark-gluon plasma in equilibrium (in the quenched approximation). We emphasize, however, that we cannot directly compare our results to these lattice results, since we consider only low invariant mass dileptons at high energy, that is, Q^μ close to the light cone (in the plasma frame), while the lattice data presented in [42, 43] are for dileptons at rest–a regime where our treatment is not valid. The comparison is further obscured by the fact that the present results have to be extrapolated to large values of the coupling, while the rationale for keeping only ladder diagrams is based on low values of the coupling.

The present results assume that the plasma is in equilibrium, and use asymptotic values for the various thermal and screening masses. They are therefore expected to be quantitatively reliable only at extremely high temperature. More realistic results for comparison with present and future experiments at RHIC and LHC could be obtained by using more realistic mass estimates, from the lattice for example, and also by relaxing the assumption of chemical equilibrium. Of course, the obtained results would be on a less firm theoretical ground but they might be phenomenologically useful.

The dilepton channel can offer complementary information to the real photon channel as a probe for formation of a quark-gluon plasma in heavy ion collisions, since the background is expected to be relatively much less important than for real photon. In this respect it would be useful to evaluate the contribution of non thermal sources of lepton pairs for comparison with the rates calculated here.

Acknowledgments

We wish to thank Peter Arnold, Dominique Schiff and Larry Yaffe for useful conversations. F.G. would like to thank the LPT/Orsay where part of this work has been performed. The work of G.M. was supported by the U.S. Department of Energy under Grant No. DE-FG03-96ER40956.

References

[1] J. Kapusta, P. Lichard and D. Seibert, *High-energy photons from quark-gluon plasma versus hot hadronic gas*, *Phys. Rev.* **D 44** (1991) 2774.

[2] R. Baier, H. Nakkagawa, A. Niegawa and K. Redlich, *Production rate of hard thermal photons and screening of quark mass singularity*, *Z. Physik* **C 53** (1992) 433.

[3] P. Aurenche, F. Gelis, R. Kobes and E. Petitgirard, *Enhanced photon production rate on the light-cone*, *Phys. Rev.* **D 54** (1996) 5274 [hep-ph/9604398].

[4] P. Aurenche, F. Gelis, R. Kobes and E. Petitgirard, *Breakdown of the hard thermal loop expansion near the light-cone*, *Z. Physik* **C 75** (1997) 315 [hep-ph/9609256].

[5] P. Aurenche, F. Gelis, R. Kobes and H. Zaraket, *Bremsstrahlung and photon production in thermal QCD*, *Phys. Rev.* **D 58** (1998) 085003 [hep-ph/9804224].

[6] D. Dutta, S.V.S. Sastry, A.K. Mohanty, K. Kumar and R.K. Choudhury, *Hard photon production from unsaturated quark gluon plasma at two loop level*, *Nucl. Phys.* **A 710** (2002) 415 [hep-ph/0104134].

[7] F.D. Steffen and M.H. Thoma, *Hard thermal photon production in relativistic heavy ion collisions*, *Phys. Lett.* **B 510** (2001) 98 [hep-ph/0103044].

[8] P. Aurenche, F. Gelis and H. Zaraket, *A simple sum rule for the thermal gluon spectral function and applications*, *J. High Energy Phys.* **05** (2002) 043 [hep-ph/0204146].

[9] P. Aurenche, F. Gelis and H. Zaraket, *Landau-Pomeranchuk-Migdal effect in thermal field theory*, *Phys. Rev.* **D 62** (2000) 096012 [hep-ph/0003326].

[10] E. Braaten and R.D. Pisarski, *Soft amplitudes in hot gauge theories: a general analysis*, *Nucl. Phys.* **B 337** (1990) 569.

[11] P. Arnold, G.D. Moore and L.G. Yaffe, *Photon emission from ultrarelativistic plasmas*, *J. High Energy Phys.* **11** (2001) 057 [hep-ph/0109064].

[12] P. Arnold, G.D. Moore and L.G. Yaffe, *Photon emission from quark gluon plasma: complete leading order results*, *J. High Energy Phys.* **12** (2001) 009 [hep-ph/0111107].

[13] P. Arnold, G.D. Moore and L.G. Yaffe, *Photon and gluon emission in relativistic plasmas*, *J. High Energy Phys.* **06** (2002) 030 [hep-ph/0204343].

[14] L.D. Landau and I.Ya. Pomeranchuk, *Limits of applicability of the theory of bremsstrahlung electrons and pair production at high-energies. (In Russian) Dokl. Akad. Nauk. SSR* **92** (1953) 535.

[15] L.D. Landau and I.Ya. Pomeranchuk, *Electron cascade process at very high-energies. (In Russian)*, *Dokl. Akad. Nauk. SSR* **92** (1953) 735.

[16] A.B. Migdal, *Bremsstrahlung and pair production in condensed media at high-energies*, *Phys. Rev.* **103** (1956) 1811.

[17] R. Baier, Y.L. Dokshitzer, S. Peigne and D. Schiff, *Induced gluon radiation in a QCD medium*, *Phys. Lett.* **B 345** (1995) 277 [hep-ph/9411409].

[18] R. Baier, Y.L. Dokshitzer, A.H. Mueller, S. Peigne and D. Schiff, *Radiative energy loss of high energy quarks and gluons in a finite-volume quark-gluon plasma*, *Nucl. Phys.* **B 483** (1997) 291 [hep-ph/9607355].

[19] R. Baier, Y.L. Dokshitzer, A.H. Mueller and D. Schiff, *Medium-induced radiative energy loss: equivalence between the BDMPS and Zakharov formalisms*, *Nucl. Phys.* **B 531** (1998) 403 [hep-ph/9804212].

[20] B.G. Zakharov, *Fully quantum treatment of the Landau-Pomeranchuk-Migdal effect in QED and QCD*, *Sov. Phys. JETP Lett.* **63** (1996) 952 [hep-ph/9607440].

[21] B.G. Zakharov, *Landau-Pomeranchuk-Migdal effect for finite size targets*, *Sov. Phys. JETP Lett.* **64** (1996) 781 [*Zh. Eksp. Teor. Fiz.* **64** (1996) 737] [hep-ph/9612431].

[22] B.G. Zakharov, *Light cone path integral approach to the Landau-Pomeranchuk-Migdal effect*, *Phys. Atom. Nucl.* **61** (1998) 838 [*Yad. Fiz.* **61** (1998) 924] [hep-ph/9807540].

[23] V.V. Lebedev and A.V. Smilga, *Anomalous damping in plasma*, *Physica* **A181** (1992) 181.

JHEP12(2002)006

[24] V.V. Lebedev and A.V. Smilga, *Spectrum of quark-gluon plasma*, *Ann. Phys. (NY)* **202** (1990) 229.

[25] M.E. Carrington and R. Kobes, *The general cancellation of ladder graphs at finite temperature*, *Phys. Rev.* **D 57** (1998) 6372 [hep-ph/9712280].

[26] M.E. Carrington, R. Kobes and E. Petitgirard, *Cancellation of ladder graphs in an effective expansion*, *Phys. Rev.* **D 57** (1998) 2631 [hep-ph/9708412].

[27] D.K. Srivastava, *Photon production in relativistic heavy ion collisions using rates with two loop calculations from quark matter*, *Eur. Phys. J.* **C 10** (1999) 487.

[28] D.K. Srivastava and B. Sinha, *Radiation of single photons from* Pb + Pb *collisions at the cern SPS and quark hadron phase transition*, *Phys. Rev.* **D 64** (2001) 034902 [nucl-th/0006018].

[29] P. Huovinen, P.V. Ruuskanen and S.S. Rasanen, *Photon emission in heavy ion collisions at the Cern SPS*, *Phys. Lett.* **B 535** (2002) 109 [nucl-th/0111052].

[30] A.K. Chaudhuri, *Single photons from* Pb + Pb *collisions at Cern SPS, QGP vs. hadronic gas*, nucl-th/0012058.

[31] A.K. Chaudhuri and T. Kodama, *Direct photons from relativistic heavy ion collisions at Cern SPS and at RHIC*, nucl-th/0203067.

[32] WA98 collaboration, M.M. Aggarwal et al., *Observation of direct photons in central 158 A GeV* ^{208}Pb +^{208} Pb *collisions*, *Phys. Rev. Lett.* **85** (2000) 3595 [nucl-ex/0006008].

[33] R. Averbeck, for the PHENIX collaboration, *Single leptons from heavy flavor decays at RHIC*, talk at Quark-Matter 2002, July 18-24 2002, Nantes, France nucl-ex/0209016;
K. Reygers, for the Phenix collaboration, *Results on photon production in Au+Au collisions at RHIC*, talk given at Quark Matter 2002, Nantes, France, 18-24 Jul 2002, nucl-ex/0209021.

[34] L.D. McLerran and T. Toimela, *Photon and dilepton emission from the quark-gluon plasma: some general considerations*, *Phys. Rev.* **D 31** (1985) 545.

[35] T. Altherr and P.V. Ruuskanen, *Low mass dileptons at high momenta in ultrarelativistic heavy ion collisions*, *Nucl. Phys.* **B 380** (1992) 377.

[36] M.H. Thoma and C.T. Traxler, *Production of energetic dileptons with small invariant masses from the quark-gluon plasma*, *Phys. Rev.* **D 56** (1997) 198 [hep-ph/9701354].

[37] P. Aurenche, F. Gelis and H. Zaraket, *Enhanced thermal production of hard dileptons by* $3 \to 2$ *processes*, *J. High Energy Phys.* **07** (2002) 063 [hep-ph/0204145].

[38] S. Catani and B.R. Webber, *Infrared safe but infinite: soft-gluon divergences inside the physical region*, *J. High Energy Phys.* **10** (1997) 005 [hep-ph/9710333].

[39] M. Le Bellac, *Thermal field theory*, Cambridge University Press, Cambridge 1996.

[40] S.V.S. Sastry, *On the variational method for lpm suppression of photon emission from quark gluon plasma*, hep-ph/0208103.

[41] W.H. Press, S.A. Teukolsky, W.T. Vetterling and B.P. Flannery, *Numerical recipes*, Cambridge University Press, Cambridge 1993.

[42] F. Karsch, E. Laermann, P. Petreczky, S. Stickan and I. Wetzorke, *A lattice calculation of thermal dilepton rates*, *Phys. Lett.* **B 530** (2002) 147 [hep-lat/0110208].

[43] F. Karsch, S. Datta, E. Laermann, P. Petreczky, S. Stickan and I.Wetzorke, *Hadron correlators, spectral functions and thermal dilepton rates from lattice QCD*, hep-ph/0209028.

JHEP12(2002)006